MULTI-SCALE CRACK PROPAGATION ANALYSIS FOR STRENGH ASSESSMENT OF POLYCRSTALINE MATERIALS

Y. Shintaku[1], K. Terada[2], J. Kato[2], T. Kyoya[1], S. Takase[2] and S. Tsutsumi[3]

[1] Department of Civil and Environmental Engineering
Tohoku University
6-6 Aoba, Aramaki, Sendai 980-8579, JAPAN
e-mail: shintaku@mm.civil.tohoku.ac.jp

[2] International Research Institute of Disaster Science
Tohoku University
6-6 Aoba, Aramaki, Sendai 980-8579, JAPAN

Jointing and Welding Research Institute
Osaka University
11-1 Mihogaoka, Ibaraki, Osaka 567-0047, JAPAN

Key words: Multi-scale analysis, Crack propagation, Crystal plasticity, Fatigue fracture, Chemical attack

Abstract. The objective of this study is to develop a method of multi-scale crack propagation analysis to assess the residual strength of the structure subjected to chemical attack. The macro-scale crack growth rate is determined by both the micro-scale cracking with plastic deformations and the change of the hydrogen concentrations. The micro-scale crack propagation is simulated by the crystal plasticity model and the cohesive zone model induced by the change of the surface energy to account for the hydrogen effect. A polycrystalline aggregate is regarded as a representative volume element (RVE) for micro-scale analyses and the macroscopic strength is estimated from this result. The macro-scale crack growth simulation is conducted using the cohesive zone model with the parameter the strength reflected the micro-scale analysis and the damage evolved by the fatigue. The proposed method enables us to simulate the crack propagation with the evaluation of fatigue and the effect of hydrogen.

1 INTRODUCTION

Cohesive zone model is widely utilized for the crack propagation analysis. The difference from the linear fracture mechanics is that the cohesive zone model modifies the

singular stress at crack tip to the more realistic nonlinear condition of material response. In this regard, Elliots [1] propose the original idea by the development of the Griffith theory [2] and introduces an attractive force per unit area between atomics. Barenblatt [4] presents more specific model to account for finite strength and then Dugdale [3] investigates the size of plastic size using a similar model, so-called strip-yield model. Needleman [5] introduces the cohesive element technique in the finite element framework for fracture study. Now the cohesive zone model becomes a popular tool for simulating fracture processes in materials and structures due to the computational convenience.

In a polycrystalline aggregate, micro crack propagation is simulated by the microscopic cohesive zone model. One of them is based on an atomic potential and provides the relationship between binding energies and separation of materials. Rice and Wang [6] employ *universal binding energy* proposed by Rose et al. [7] to derive their model. They introduce the surface energy in the frame work of Griffith theory and discuss the change of the intergranular fracture by the chemical effect. Rimoli and Ortiz [8] simulate the propagation of the intergranular hydrogen-assisted crack using the similar cohesive zone model and the grain boundary diffusion of the hydrogen. Recently, the parameter of cohesive zone model is investigated actively using modular dynamics [9] and discrete dislocation modeling [10]. On the other hand, numerous cohesive zone models are proposed in macro-scale and various fracture process in various materials are simulated using them. For example, Hillerborg et al. [11] simulate quasi-brittle fracture in concrete using a linear softening model. Jin et al. [12] propose a phenomenological traction-based cohesive zone model for metal-ceramic functionally graded materials. Fatigue fracture is studied by the introduction of the damage model into cohesive zone model. Nugyen and Reppeto [13] propose this kind of cohesive zone model and compare with the experimental data inside the Paris regime. The fracture process outside this regime is simulated, such as short cracks and overloading. Bouvard and Chaboche et al. [14] develope the cohesive zone coupled with creep fracture.

The present work provides multi-scale crack propagation analysis by the estimation of macroscopic fracture parameters from the micro-scale analysis. A polycrystalline aggregate is regarded as a representative volume element (RVE) for micro-scale analyses. We utilize the cohesive zone model based on the atomic potential and introduce impurity-dependency according to the Griffith theory. The parameter of macroscopic one is investigated from the microscopic analysis. Moreover, the damage variable is added to this macroscopic cohesive zone model and the fatigue crack probation is simulated with the parameter.

2 CRYSTAL PLASTICITY MODEL

In this section, crystal plasticity model, which is utilized as the microscopic material response, is explained.

2.1 Multiplicative decomposition of deformation gradient: Elasticity and plasticity deformation

The total deformation gradient is assumed to be decomposed into the two parts as shown in eq. (1). One is the elastic deformation due to distortion of crystal lattices, and the other is plastic deformation due to crystallographic slip,

$$\boldsymbol{F} = \boldsymbol{F}^{\mathrm{e}}\boldsymbol{F}^{\mathrm{p}}, \tag{1}$$

where $\boldsymbol{F}^{\mathrm{e}}$ is the elastic deformation gradient and $\boldsymbol{F}^{\mathrm{p}}$ is the plastic deformation gradient, respectively. The velocity gradient is expressed as the additive decomposition as follows:

$$\boldsymbol{l} := \dot{\boldsymbol{F}}\boldsymbol{F}^{-1} = \boldsymbol{l}^{\mathrm{e}} + \boldsymbol{l}^{\mathrm{p}}, \tag{2}$$

where the velocity gradients due to elastic deformation $\boldsymbol{l}^{\mathrm{e}}$ and crystallographic slip and $\boldsymbol{l}^{\mathrm{p}}$ have respectively been defined as

$$\begin{cases} \boldsymbol{l}^{\mathrm{e}} := \dot{\boldsymbol{F}}^{\mathrm{e}}\boldsymbol{F}^{\mathrm{e}-1} \\ \boldsymbol{l}^{\mathrm{p}} := \boldsymbol{F}^{\mathrm{e}}\dot{\boldsymbol{F}}^{\mathrm{p}}\boldsymbol{F}^{\mathrm{p}-1}\boldsymbol{F}^{\mathrm{e}-1}. \end{cases} \tag{3}$$

Further, denoting the symmetric and antisymmetric components of the second-order tensor $\bullet$ respectively by $\mathrm{sym}[\bullet]$ and $\mathrm{skw}[\bullet]$, we decompose the rate-of-deformation tensor $\boldsymbol{d}$ and the spin tensor $\boldsymbol{w}$ additively into the corresponding elastic and plastic components as follows:

$$\boldsymbol{d} := \mathrm{sym}[\boldsymbol{l}] = \boldsymbol{d}^{\mathrm{e}} + \boldsymbol{d}^{\mathrm{p}} := \mathrm{sym}[\boldsymbol{l}^{\mathrm{e}}] + \mathrm{sym}[\boldsymbol{l}^{\mathrm{p}}], \tag{4}$$

$$\boldsymbol{w} := \mathrm{skw}[\boldsymbol{l}] = \boldsymbol{w}^{\mathrm{e}} + \boldsymbol{w}^{\mathrm{p}} := \mathrm{skw}[\boldsymbol{l}^{\mathrm{e}}] + \mathrm{skw}[\boldsymbol{l}^{\mathrm{p}}]. \tag{5}$$

2.2 Flow rule for crystallographic slip

Let $\boldsymbol{s}_0^{(\alpha)}$ be the unit vector that defines the slip direction and $\boldsymbol{m}_0^{(\alpha)}$ be the unit vector that defines the normal direction of the slip surfaces at the initial or reference configuration of a certain slip system α. On the assumption that the crystal lattice is not distorted by the slip-deformations, the vectors of slip and normal directions, which are assumed to be mutually-perpendicular, are defined as follows:

$$\boldsymbol{s}^{*(\alpha)} = \boldsymbol{F}^{\mathrm{e}}\boldsymbol{F}^{\mathrm{t}}\boldsymbol{s}_0^{(\alpha)}, \quad \boldsymbol{m}^{*(\alpha)} = \boldsymbol{m}_0^{(\alpha)}\boldsymbol{F}^{\mathrm{t}-1}\boldsymbol{F}^{\mathrm{e}-1}. \tag{6}$$

Also, the resolved shear stress on slip system α is defined as

$$\tau^{(\alpha)} = (\boldsymbol{s}^{*(\alpha)} \otimes \boldsymbol{m}^{*(\alpha)}) : J\boldsymbol{\sigma}, \tag{7}$$

where $\boldsymbol{\sigma}$ is the Cauchy stress and J is the determinant of $\boldsymbol{F}$. Since the overall plastic power is equivalent to the summation of the plastic powers of all the slip systems, the following relationship is postulated:

$$J\boldsymbol{\sigma} : \boldsymbol{l}^{\mathrm{p}} = \sum_{\alpha=1}^{n} \tau^{(\alpha)} \dot{\gamma}^{(\alpha)} \tag{8}$$

where n is the number of slip systems of the crystal lattice of a hcp metal, $\boldsymbol{l}^{\mathrm{p}}$ is the plastic deformation gradient defined in eq. (2) and $\dot{\gamma}^{(\alpha)}$ is the slip rate in slip system α. By the substitution of eq. (7) to this identity, the plastic velocity gradient can be related to the slip rate as

$$\boldsymbol{l}^{\mathrm{p}} = \sum_{\alpha=1}^{n} \left(\boldsymbol{s}^{*(\alpha)} \otimes \boldsymbol{m}^{*(\alpha)} \right) \dot{\gamma}^{(\alpha)}, \tag{9}$$

which is the flow rule for a crystal plasticity model. With this definition, the plastic rate-of-deformation tensor and the plastic spin tensor of the crystallographic slip can be expressed as follows:

$$\boldsymbol{d}^{\mathrm{p}} = \sum_{\alpha=1}^{n} \boldsymbol{\mu}^{(\alpha)} \dot{\gamma}^{(\alpha)}, \quad \boldsymbol{w}^{\mathrm{p}} = \sum_{\alpha=1}^{n} \boldsymbol{\omega}^{(\alpha)} \dot{\gamma}^{(\alpha)}. \tag{10}$$

Here, $\boldsymbol{\mu}^{(\alpha)}$ and $\boldsymbol{\omega}^{(\alpha)}$ are the symmetric and anti-symmetric components of $(\boldsymbol{s}^{*(\alpha)} \otimes \boldsymbol{m}^{*(\alpha)})$, which are defined as

$$\boldsymbol{\mu}^{(\alpha)} := \mathrm{sym}[\boldsymbol{s}^{*(\alpha)} \otimes \boldsymbol{m}^{*(\alpha)}], \quad \boldsymbol{\omega}^{(\alpha)} := \mathrm{skw}[\boldsymbol{s}^{*(\alpha)} \otimes \boldsymbol{m}^{*(\alpha)}]. \tag{11}$$

2.3 Slip rate

Although various models for crystallographic slip have been proposed in the literature, the following visco-plastic evolution law of exponential form, which was originally presented by Asaro et al. [15], is employed in this study:

$$\dot{\gamma}^{(\alpha)} := \dot{a} \left| \frac{\tau^{(\alpha)}}{g^{(\alpha)}} \right|^{n^{\mathrm{v}}} \mathrm{sign} \left(\frac{\tau^{(\alpha)}}{g^{(\alpha)}} \right), \tag{12}$$

where $\dot{a}$ is the reference slip rate, $g^{(\alpha)}$ is the slip resistance of slip system α and n^{v} a parameter that controls the strain rate dependency. The relevant hardening law, which is the evolution equation of slip resistance $g^{(\alpha)}$, is given as

$$\dot{g}^{(\alpha)} := \sum_{\beta=1}^{n} h_{\alpha\beta} \dot{\gamma}^{(\beta)}, \tag{13}$$

where $h_{\alpha\beta}$ represents the hardening moduli. In this study, we employ the following hardening function presented by Asaro et al. [15]:

$$\begin{cases} h_{\alpha\alpha} := h_0 \mathrm{sech}^2 \left| \dfrac{h_0\gamma}{\tau_s - \tau_0} \right| \\ h_{\alpha\beta} := qh_{\alpha\alpha} \quad (\alpha \neq \beta), \end{cases} \tag{14}$$

where $h_{\alpha\alpha}$ (no sum) and $h_{\alpha\beta}$ are the self-hardening and latent hardening moduli with q being the ratio of the latter to the former. Also, h_0, τ_0 and τ_s are the initial hardening modulus, the initial CRSS and the stage-I (saturation) stress, respectively. Here, each hardening modulus is assumed to be a function of the total amount of accumulated slip, defined as:

$$\gamma := \sum_{\alpha=1}^{n} \int_0^t |\dot{\gamma}^{(\alpha)}| \mathrm{dt}. \tag{15}$$

3   COHESIVE ZNONE MODEL

In this section, micro-scale and macro-scale cohesive zone models are expressed respectively. Microscopic model is formulated from atomic potential and then the damage variable is introduced to macroscopic model within the framework of thermodynamics.

3.1   Microscopic model

Rose et al. [7] gather numerous results of the first-principle calculations and analyze the cohesive energy of various kinds of atomics, and then present the relationship of the binding energy as a function of separation which is called *universal binding energy* Ψ_m as follows,

$$\Psi_\mathrm{m} = -(1 + l)\exp(-l), \tag{16}$$

where l is the scaled separation associated with the Thomas-Fermi screening length. Rice and Wang [6] propose the exponential type of cohesive zone model from this relationship. As the additional revision, Needleman [5] introduce the cohesive potential and expresses exponential potential model. We also assume that the cohesive potential is the exponential function and it is defined by

$$\Psi_\mathrm{m} = -A_\mathrm{m}\boldsymbol{\delta}_{\mathrm{m,c}} \left(1 + \frac{\boldsymbol{\delta}_\mathrm{m}}{\boldsymbol{\delta}_{\mathrm{m,c}}} \right) \exp\left(-\frac{\boldsymbol{\delta}_\mathrm{m}}{\boldsymbol{\delta}_{\mathrm{m,c}}} \right), \tag{17}$$

where $\boldsymbol{\delta}_\mathrm{m}$ is the separation displacement, $\boldsymbol{\delta}_{\mathrm{m,c}}$ is the critical state of $\boldsymbol{\delta}_\mathrm{m}$ and A_m is the initial modulus. The normal traction to crack surface cohesive is given by the differential equation of the potential,

$$\boldsymbol{T}_\mathrm{m} = \frac{\partial \Psi_\mathrm{m}}{\partial \boldsymbol{\delta}_\mathrm{m}} = A_\mathrm{m}\frac{\boldsymbol{\delta}_\mathrm{m}}{\boldsymbol{\delta}_{\mathrm{m,c}}}\exp\left(-\frac{\boldsymbol{\delta}_\mathrm{m}}{\boldsymbol{\delta}_{\mathrm{m,c}}} \right). \tag{18}$$

5

This interfacial cohesive traction $\boldsymbol{T}_{\mathrm{m}}$ initially increases until the interface separation $\boldsymbol{\delta}_{\mathrm{m}}$ becomes $\boldsymbol{\delta}_{\mathrm{m,c}}$ as shown in **Fig. 3**, and then it decreases asymptotically to zero. In the Griffith theory, the critical energy release rate G_{c} given by

$$G_{\mathrm{c}} = \int_0^\infty \boldsymbol{T}_{\mathrm{m}} d\delta = A_{\mathrm{m}}\boldsymbol{\delta}_{\mathrm{c}} = 2\omega_{\mathrm{c}}, \tag{19}$$

where ω_{c} is the critical energy per unit required to make new crack surface. Irwin and Orowan [17] assumed that ω_{c} is devided into two parts, the surface energy ω_{s} and the plastic work ω_{p} ($\omega_{\mathrm{c}} = \omega_{\mathrm{s}} + \omega_{\mathrm{p}}$). On the other hand, Jokl et al. [18] demonstrate these two parts interact with each other; the increase of ω_{s} involves the rapid increase of ω_{p}. Rice et al. [6] and Rimoli et al. [8] allow the existence of ω_{p} but ω_{p} is neglected ($\omega_{\mathrm{c}} \approx \omega_{\mathrm{s}}$), and we also utilize same formulation.

Equation (19) is substituted in the cohesive potential (eq. (17)) and traction (eq. (18)) and these are expressed by the surface energy ω_{s}. The potensial and traction can be rewritten as

$$\Psi_{\mathrm{m}} = -2\omega_{s} \left(1 + \frac{\boldsymbol{\delta}_{\mathrm{m}}}{\boldsymbol{\delta}_{\mathrm{m,c}}}\right) \exp\left(-\frac{\boldsymbol{\delta}_{\mathrm{m}}}{\boldsymbol{\delta}_{\mathrm{m,c}}}\right), \tag{20}$$

$$\boldsymbol{T}_{\mathrm{m}} = \frac{\partial \Psi_{\mathrm{m}}}{\partial \boldsymbol{\delta}_{\mathrm{m}}} = \frac{2\omega_{s}}{\boldsymbol{\delta}_{\mathrm{m,c}}} \left(\frac{\boldsymbol{\delta}_{\mathrm{m}}}{\boldsymbol{\delta}_{\mathrm{m,c}}}\right) \exp\left(-\frac{\boldsymbol{\delta}_{\mathrm{m}}}{\boldsymbol{\delta}_{\mathrm{m,c}}}\right). \tag{21}$$

The surface energy ω_{s} is changed by the chemical attack and the hydrogen in particular involves the decreases of ω_{s}. Jiang et al. [19] investigate the influence of hydrogen and Rimoli and Ortiz. [8] approximate this data by quadric equation as shown Fig. 2, and it gives,

$$\omega_{\mathrm{s}}(\theta) = \left(1 - 1.0467\theta + 0.1687\theta^2\right)\omega_{\mathrm{s}0}, \tag{22}$$

where $\theta = \Gamma/\Gamma_{\mathrm{s}}$ is the coverage, Γ is the surface concentration, Γ_{s} is the saturation value, and $\omega_{\mathrm{s}0}$ is the surface energy when $\Gamma = 0$. By the decrease of the surface energy ω_{s}, maximum value of the cohesive traction is decrease as shown in Fig. 1.

3.2 Macroscopic model

The various fracture process in each material is simulated by each cohesive zone model based on the phenomenological theory. One of the famous macroscopic cohesive zone models is the exponential type such as eq. (17) and (18). In the next section, we estimate the macroscopic parameter of the cohesive zone model from the micro boundary value problem (BVP). Fatigue crack propagation is simulated using the cohesive zone model with the damage theory. In this study, we apply the damage variable D to the cohesive potential eq. (17),

$$\Psi_{\mathrm{M}} = -(1-D) A_{\mathrm{M}}\boldsymbol{\delta}_{\mathrm{M,c}} \left(1 + \frac{\boldsymbol{\delta}_{\mathrm{M}}}{\boldsymbol{\delta}_{\mathrm{M,c}}}\right) \exp\left(-\frac{\boldsymbol{\delta}_{\mathrm{M}}}{\boldsymbol{\delta}_{\mathrm{M,c}}}\right). \tag{23}$$
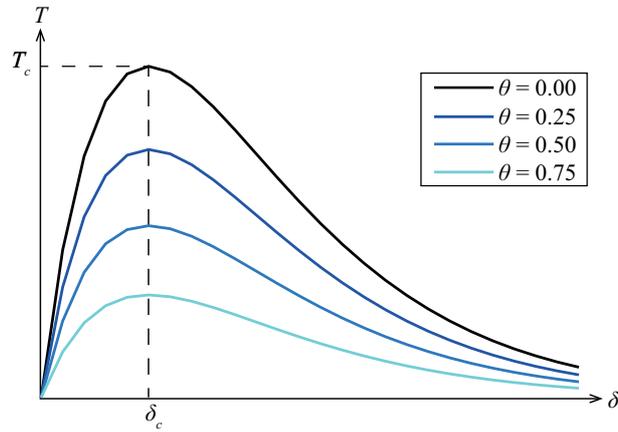
Figure 1: Comparison of the cohesive traction curves with hydrogen converge fraction
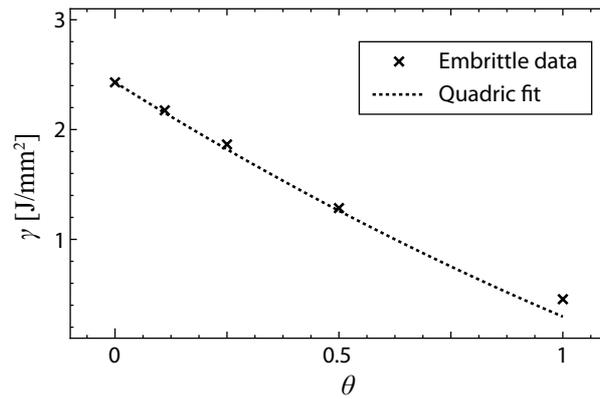
Figure 2: Surface energy with hydrogen converge fraction

where the lower index M indicates the variable at macroscopic level in this section. The macroscopic cohesive traction is given by

$$\boldsymbol{T}_M = \frac{\partial \Psi_{\mathrm{M}}}{\partial \boldsymbol{\delta}_{\mathrm{M}}} = (1 - D) A_{\mathrm{M}} \left(\frac{\boldsymbol{\delta}_{\mathrm{M}}}{\boldsymbol{\delta}_{\mathrm{M,c}}} \right) \exp \left(-\frac{\boldsymbol{\delta}_{\mathrm{M}}}{\boldsymbol{\delta}_{\mathrm{M,c}}} \right)_{.} \tag{24}$$

The thermodynamic force Y associated with the damage variable can be written as the derivative of eq. (23) and means the dissipation of the cohesive potential by the damage progress,

$$Y = -\frac{\partial \Psi_{\mathrm{M}}}{\partial D} = -A_{\mathrm{M}} \boldsymbol{\delta}_{\mathrm{M,c}} \left(1 + \frac{\boldsymbol{\delta}_{\mathrm{M}}}{\boldsymbol{\delta}_{\mathrm{M,c}}} \right) \exp \left(-\frac{\boldsymbol{\delta}_{\mathrm{M}}}{\boldsymbol{\delta}_{\mathrm{M,c}}} \right)_{.} \tag{25}$$

In this model, the damage begins after then Y exceeds the threshold value Y_{th} and the damage accumulates as crack opening increases under loading ($\dot{Y} \geq 0$),

$$\dot{D} = C(1 - D)^m \langle \sqrt{Y} - \sqrt{Y_{\mathrm{th}}} \rangle^n \| \frac{\dot{\boldsymbol{\delta}}_{\mathrm{M}}}{\boldsymbol{\delta}_{\mathrm{M,c}}} \| \quad (\text{if} \quad \dot{Y} \geq 0), \tag{26}$$

$$\dot{D} = 0 \qquad \qquad (\text{otherwise}), \tag{27}$$

where C, m, and n are the material constants. **Fig. 3** shows a sketch for the macroscopic model response under cyclic loading. The cohesive traction $\boldsymbol{T}_{\mathrm{M}}$ goes back to the origin with linear path under unloading condition while it shows nonlinear path under reloading.
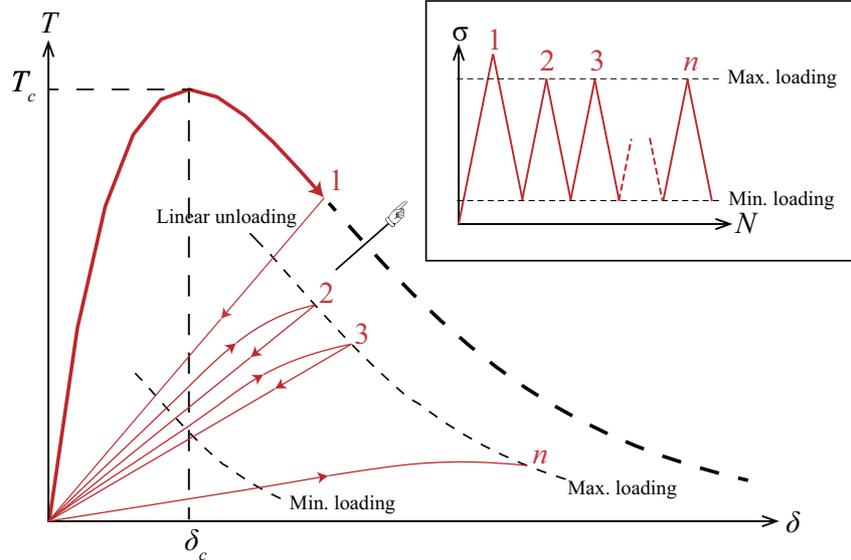
Figure 3: $T_M - \delta_M$ cohesive traction under cyclic loading

4 Numerical example

The RVE shown as **Fig. 4** is used for the micro-scale analysis displacement is distributed on the upper and lower edge of the plate and left side of the. The right side of the plate is fixed to x-direction and movable to y-direction. The RVE is assumed to be a stainless alloy, which consists of 14 crystal grains. The material properties are given in **Fig. 4**. The cohesive zone is given in the crystal grain boundary and the parameter is assumed as $\boldsymbol{\delta}_{m,c} = 0.003[\text{mm}]$. The effect of the hydrogen is calculated as the following ratio of the surface concentration; $\theta = 0.0, 0.2, 0.4$. **Fig. 5** shows the relationship between the traction and the displacement associated with the constrain point. The maximum traction decreases by the effect of hydrogen and may be smaller than actual material response because of the neglect of ω_p. We assume that the whole response of the RVE is similar with the response of the macroscopic cohesive zone model. The macroscopic $T_{\text{M,c}}$ and $\delta_{\text{M,c}}$ are estimated from this load displacement curve using the renormalization procedure, such as Nuguyen and Ortiz [20].

The fatigue crack growth problem is analyzed through 1CT specimen under the assumption of the linear elastic condition. Considering the symmetry of the problem, the computational domain can be restricted to the quarter model as shown in **Fig. 6**. The parameter of the fracture toughness is calculated from the micro-scale result and the fatigue parameter is estimated as shown **Fig. 6**. The relationship between crack growth length and the number of cycles is shown as **Fig. 7** and the crack growths rapidly by the effect of the hydrogen.

$\varepsilon = 1.0\ [\%]$

Young's modulus:	$E = 206[\text{GPa}]$
Poisson's ratio:	$\nu = 0.3$
Reference slip rate:	$\dot{a} = 0.001$
Strain rate dependency:	$n^Y = 30$
Initial hardening modulus:	$h_0 = 220$
Stage-I stress :	$\tau_s = 300[\text{MPa}]$
Initial CRSS :	$\tau_0 = 93[\text{MPa}]$
Ratio of the hardening modulus:	$q_{\alpha\beta} = 1$
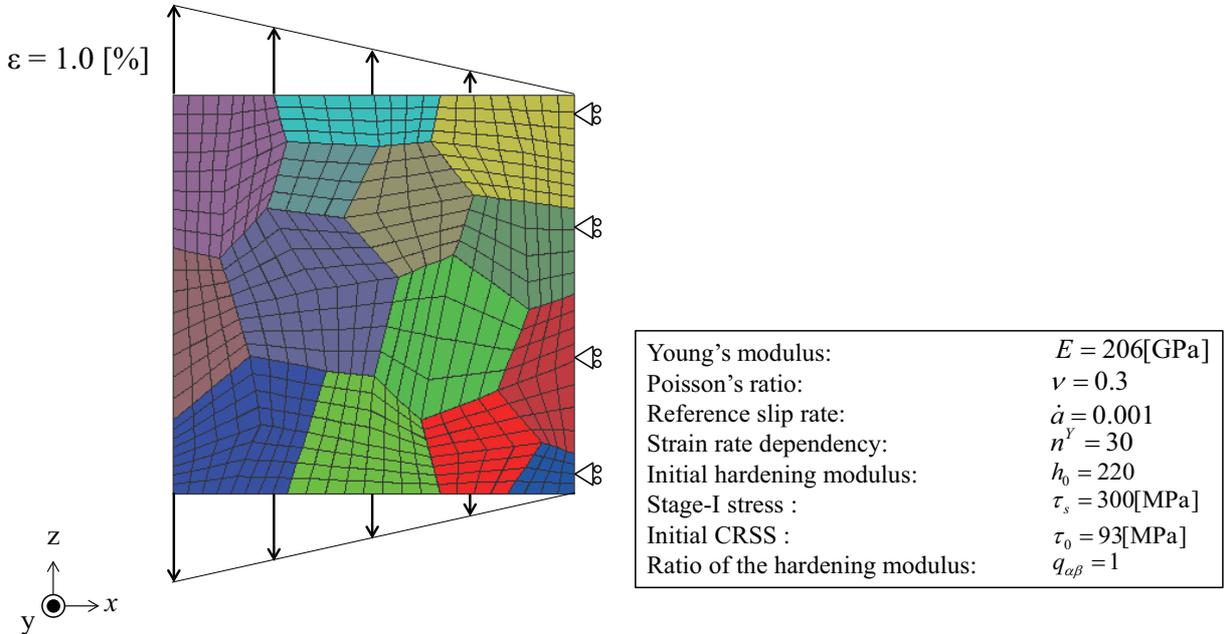
Figure 4: The micro-scale numerical model and conditions

9
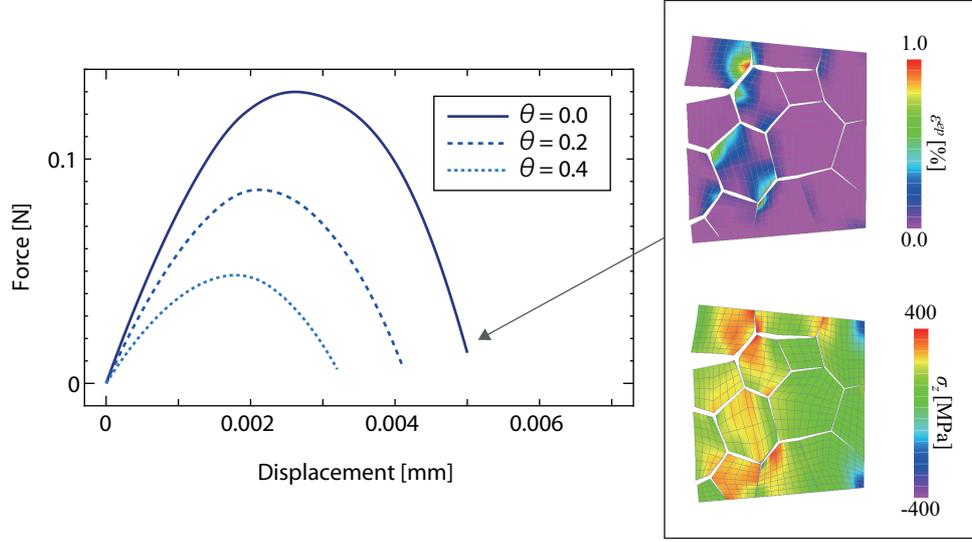
Figure 5: Relationship between the transition and the displacement in the micro-scale analysis
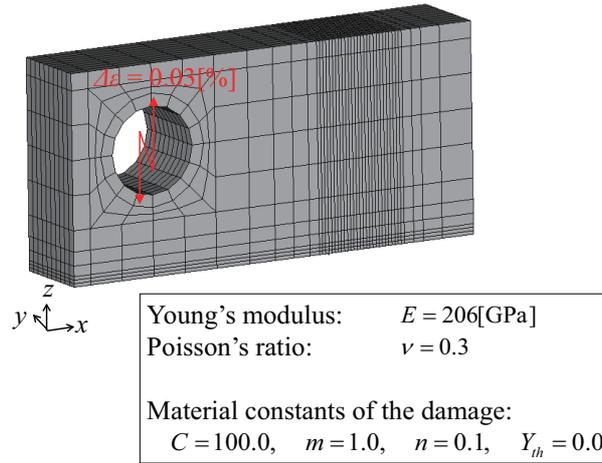
Figure 6: Macro-scale numerical model and conditions

5   CONCLUSIONS

- We estimated the macroscopic strengh of the polycrystalline structure material from the micro-scale analysis. The change of it was calculated from the decrease of the surface energy because of the hydrogen, although we need to reconsider of the plasic work ω_p.

- The fatigue crack propagation considering the effect of hydrogen was simulated using the parameter evaluated from the micro-scale analysis.
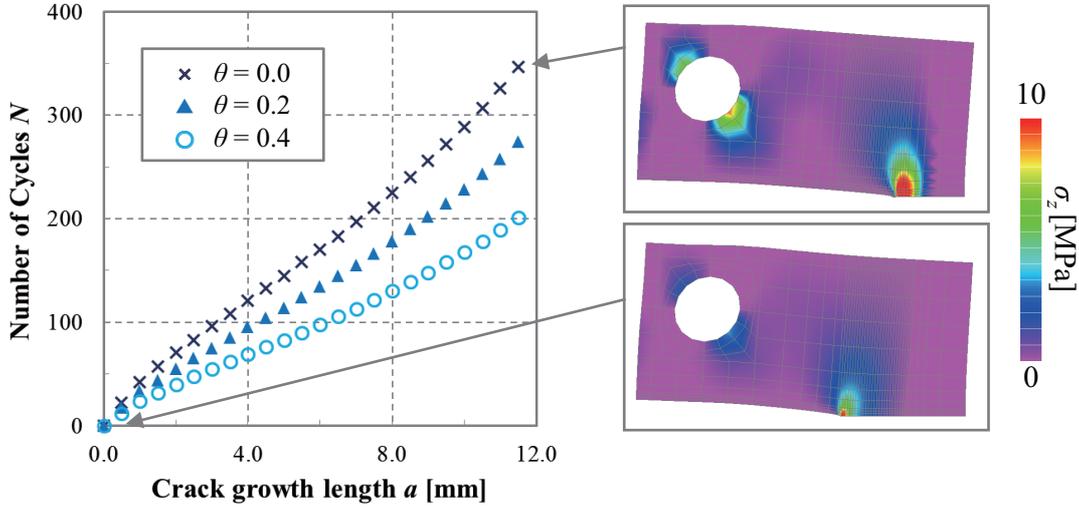
Figure 7: Crack growth lengh under cylcic loading

ACKNOWLEDGEMENT

REFERENCES

[1] Elliots, H.A. *Analysis of the conditions for rupture due to griffith crack*. Proc. Phys. Soc. (1947) **59**: 208–223.

[2] Griffith, A.A. *The Phenomena of Rupture and Flow in Solids. Phil. Trans. Roy. Soc. A(1920)* **221**: 163–198.

[3] Dugdale, D.S. *Yield in Steel Sheets Containing Slits. J. Mech. Phys. Solids (1960)* **8**: 100–104.

[4] Barenblatt, G.I. *The Mathematical Theory of Equilibrium Cracks in Brittle Fracture. Adv. Appl. Mech.* (1962) Vol. VII, Academics Press, 55–129.

[5] Needleman, A. *A continuum model for void nucleation by inclusion debonding. J. Appl. Mech.* (1987) **54**: 525–531.

[6] Rice, J. and Wang, J. *Embrittlement of interfaces by solute segregation. Mater. Sci. Eng.* (1989) **A102**: 23–40.

[7] Rose, J.H. and Smith, J.R., *Universal binding energy curves for metals and bimetallic interfaces. Phys. Rev. Lett.* (1981) **47**: 675–678.

11

[8] Rimoli, J.J. and Ortiz, M. *A three dimensional multiscale model of intergranular hydogen-assisted cracking. Philos. Mag.* (2010) **90**: 2939–2963.

[9] Yamakov, V., Saether, E., Phillips, D.R. and Glaessgen, E.H. *Molecular-dynamics simulation-based cohesive zone representation of intergranular fracture processes in aluminum. J. Mech. Phys. Solids.* (2006) **54**: 1899–1928.

[10] Deshpande, V.S., Neddleman, A. and Van der Giessen, E. *Discrete dislocation modeling of fatigue crack propagation. Acta. Materialia.* (2002) **50**: 831–846.

[11] Hillerborg, A., Modeer, M. and Petersson, P.E. *Analysis of crack formation and crack growth in concrete by mean of fracture mechanics and finite element. Cem. Concr. RE.* (1976) **6**: 773–781.

[12] Jin, A.H., Paulino, G. H., and Dodds, R. H., Jr. *Cohesive fracture modeling of elastic-plastic crack growth in functionally graded materials. Eng. Fract. Mech.* (2003) **70**: 1885–1912.

[13] Nguyen, O., Reppeto, R. A., Ortiz, M., and Radovitzky R.A. *A cohesive model of fatigue crack growth. Int. J. Fatigue* (2001) **110**: 351–369.

[14] Bouvard, J.L., Chaboche, J.L., Feyel, F. and Gallerneau, F. *A cohesive zone model for fatigue and creep-fatigue crack growth. Int. J. Fatigue* (2009) **53**: 1193–1196.

[15] Asaro, J.R. *Crystal plasticity. J. Appl. Mech.* (1983) **50**, 921–934.

[16] Iwin, G.R. *Fracture dynamics. Fract. Meta.* (1948) ASM, Cleveland, OH, 147–166.

[17] Orowan, E. *Fracture and Strength of Solids. Report on Progress in Physics* (1483) Vol. XII, 185.

[18] Jokl, M.L., Viek, V. and McMahon Jr, C.J. *Material rate dependence and localized deformation in crystalline solids. Acta. Metall.* (1980) **28**, 1479–1488.

[19] Jiang, E.A. and Carter, E.A. *First principles assessment of ideal fracture energies of materials with mobile implications for hydrogen embrittlement of metals. Acta. Meter.* (2004) **52**, 4801–4807.

[20] Nguyen, O. and Ortiz, M. *Coarse-graining and renormalization of atomistic binding relations and universal macroscopic cohesive behavio. J. Mech. Phys. Solids.* (2002) **50**: 1727–1741.